Solid Freeform Fabrication 2019: Proceedings of the 30th Annual International
Solid Freeform Fabrication Symposium – An Additive Manufacturing Conference
Reviewed Paper

LASER SINTERING OF PINE/POLYLATIC ACID COMPOSITES

Hui Zhang[1], David L. Bourell[2*], Yanling Guo[1*], Jian Li[1], Xiaodong Zhang[1], Yu Zhuang[1] and Zhipeng Li[3]

[1.] College of Mechatronics Engineering, Northeast Forestry University, Harbin, China, 150040
[2.] Laboratory for Freeform Fabrication, The University of Texas at Austin, Austin, TX, USA 78712
[3.] College of Traffic, Northeast Forestry University, Harbin, China, 150040
*. Correspondence: dbourell@mail.utexas.edu
nefugyl@hotmail.com

Abstract

A new powder feedstock composed of sustainable and degradable biomass composite material was proposed for laser sintering technology in this research. This biomass mixture, abbreviated P-PLA, is made up of mechanically mixed polylactic acid (PLA) powder and pine powder. The proper processing parameters were determined based on the component thermal behavior and laser sintering testing: processing temperature 130-135°C, laser power 20-24 W, scan spacing 0.1-0.2 mm, scan speed 1.6-2.2 m/s and layer thickness 0.2mm. Laser-sintered P-PLA parts exhibited much better mechanical properties compared with pine/polyethersulfone copolyester (P-CoPES) wood-plastic composite, with tensile strength 34-200% higher and flexural strength 92-246% higher than values for laser-sintered P-CoPES. Results reveal that pine powder loading can reduce the shrinkage and deformation of laser-sintered P-PLA parts. Shrinkage decreased from 4% to 0.31-2.27% in the XY plane and from 3.25% to 0.13-2.25% in the Z direction.

Keywords: Laser Sintering, Biomass Composites, Pine-Polylactic acid, Mechanical properties, Microstructures, Dimensional accuracy

1. Introduction

Laser sintering (LS), as a type of additive manufacturing (AM) technologies (also known as 3D Printing), is a powder-based additive-layer manufacturing process [1, 2]. Due to its processing flexibility and high efficiency [3], LS has gained traction in various fields including industrial manufacturing, aerospace, automobile, creative arts, biomedicine and so on [4, 5]. Up to now, polymeric matrix, metallic matrix and ceramic matrix are the common LS materials [6]. However, the high costs of machines, materials and maintenance pose an obstacle to a wider adoption of LS technology [7]. Meanwhile, there is a pressing need for the progression of LS to extend the diversity of materials available, especially sustainable and low-priced applications, due in part to a growing concern respecting energy usage and environmental issues [8].

Polylactic acid (PLA), deriving from renewable agricultural sources, is compostable, biodegradable and biocompatible. It is recognized as an environmentally-friendly thermoplastic [9]. Respecting its application in AM technologies, to a large extent, PLA and PLA-based composites are prepared as the feedstock of fused deposition modeling (FDM) [10-12]. Only a small proportion of PLA and its composites or modified materials are developed for other AM technologies. For example, Patricio et al.[13] fabricated PLA/PCL scaffolds for tissue engineering

with a biomanufacturing device, which showed improved biological and mechanical properties. Tiziano Serra[14] studied the plasticizing effect of PEG on PLA-based blends used for the fabrication of 3D-direct-printed scaffolds for tissue engineering applications, including the surface, geometrical, structural changes and modulation of the degradation rate of PLA-based 3D printed scaffolds. Since PLA is still not commercially available in a powder form with a size below 100 μm, it is hard to control thermal deformation of PLA caused by instantaneous laser energy within an acceptable range. A limited number of studies are focused on LS of PLA. K. F. Leong [15] built a porous drug delivery device by laser sintering of PLLA and examined the influence of critical LS process parameters on the dense wall formation and the control of the parts' porous microstructure. Tan et al. [16] applied LS technique to fabricate PLA scaffold specimens, which were examined using a Scanning Electron Microscope (SEM), but without measuring the material's mechanical properties. Zhou et al.[17] successfully fabricated a porous bone TE scaffold (**Figure 1** (a)) with PLLA/carbonated hydroxyapatite nanocomposite via LS. Jiaming Bai et al.[18] studied the effect of the addition of nanoclay on the thermal and flexural properties of laser-sintered PLA parts, and the laser-sintered PLA/nanoclay parts (**Figure 1** (b)) exhibited an improvement in flexural modulus compared with neat PLA.

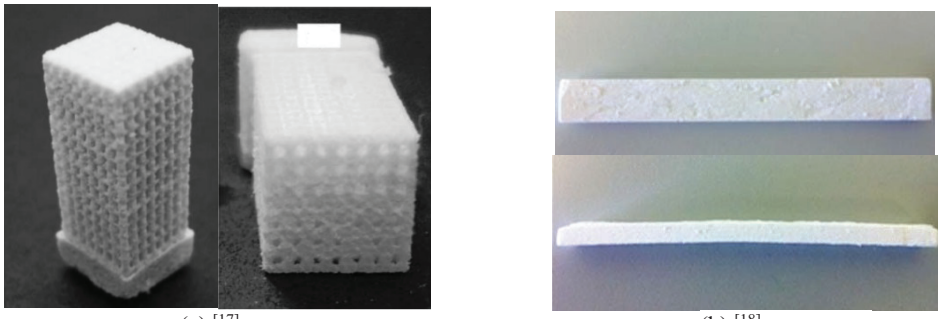

(a) [17] (b) [18]

Figure 1 Laser-sintered parts of PLA-based composites

The development of natural fiber-reinforced polymer composites using for additive manufacturing is gaining more attention [19-21]. Natural fibers, such as wood, bamboo, jute, and nut fiber, shows many advantages, including that it is biodegradable and inexpensive as well as it has relative low density but high acoustic damping [22]. A new kind of biodegradable wood-plastic composite used for LS is proposed in this research, which consists of pine powder and PLA 3052D, abbreviated P-PLA here. Pine powder acted as the filler to improve the LS formability of PLA powder, which was also intended to decrease the shrinkage and deformation of the material during LS processing. The study mainly focused on investigating the LS fabricability of P-PLA composite and the performance of laser-sintered P-PLA parts. Proper processing parameters for laser sintered neat PLA and P-PLA composites were obtained based on single-layer LS experiments and material thermal properties. The thermal behavior and the melt fluidity of neat PLA and P-PLA composites of different pine loadings were measured. The effect of pine loading on the mechanical properties, dimensional accuracy and microstructure were investigated and analyzed. The mechanical properties of laser- sintered P-PLA parts and P-CoPES (PES copolyester) parts were compared.

2. Materials and Methods

2.1 Preparation of P-PLA

The pine powder came from the waste of Mongolian Scotch pine and was purchased from Jinye Wood-fiber Factory of Xingtai Development Zone in China. Cost was $0.5/kg, and the

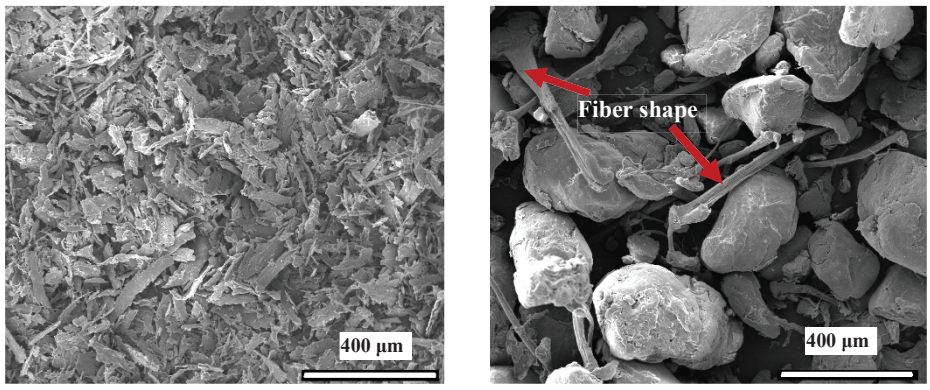

(a) Pine powder (b) PLA 3052D powder

Figure 2 Microstructures of Ingredients of P-PLA composites (× 100 times)

powder was light yellow. The particle size of most of the pine powder was smaller than 96 μm, obtained by ultrasonic oscillating sieving, with an apparent density of roughly 0.22 g/mm^3. The image in **Figure 2** (a) shows the long-flake microstructure of the pine powder observed using scanning electron microscopy (SEM).

PLA, Ingeo™ 3052D (Injection-molding grade PLA type) supplied in pellet form by NatureWorks LLC, was crushed cryogenically into powders by eSUN (Shenzhen, China). PLA 3052D was almost poly L-lactic acid (PLLA) with D-lactide contents of 4%. Cost was $20/kg, and the powder was white. The density of loose PLA powder used in this work was about 0.63 g/cm^3. However, it is difficult to obtain spherical and subglobose PLA powders by comminution due to its tacky nature [23]. As a result, the microstructure of the PLA particulate was irregular in size and shape as shown in **Figure 2** (b). Some powder was pulled into long fibers, which led to inferior flowability during the powder spreading processing by the device's roller.

Before the preparation of P-PLA composites, the pine powder was dehydrated at 60°C for 8 hours in an incubator to lower the moisture content. PLA 3052D powder was dried at 55°C for 6 hours. To assure even thermal exposure, both the pine powder and PLA 3052D powder were stirred at 2 hours intervals. The dried pine powder and PLA 3052D powder were put into a high-speed mixer and mechanically mixed below 45°C in different mass ratios. They were initially mixed for 15 min at a low speed of 750 RPM and then for 5 min at a high speed of 1500 RPM. Finally,

Figure 3 Samples of PLA 3052D, P-PLA composites and neat pine powder

different P-PLA composites with 5-40 wt.% pine loading were prepared. The neat PLA powder, neat pine powder, and some P-PLA samples are shown in **Figure 3**.

2.2 Laser sintering of P-PLA

Laser sintering (LS) experiments were carried on using an AFS-360 rapid prototyping machine (**Figure 4** (a)) fabricated by Longyuan AFS Co., Ltd. with a build chamber of 360×360×500 mm^3. The essential parameters of the machine include a CO_2 laser with a wavelength of 10.6 μm, maximum laser power of 55 W, and laser beam diameter equal to 0.4 mm.

LS tests of neat PLA powder were carried out before the PLA composite experiments to investigate the feasibility of processing PLA 3052D. Based on thermal properties of materials and 5-layer LS tests of P-PLA composites (in **Figure 4** (b)), proper process parameters of LS for PLA 3052D and P-PLA composites were established: preheating temperature 135-140°C for 2 hours, processing temperature 130-135°C, the laser power 20-24 W, scan speed 1.6-2.2 m/s, scan spacing 0.1-0.2 mm and layer thickness 0.2 mm.

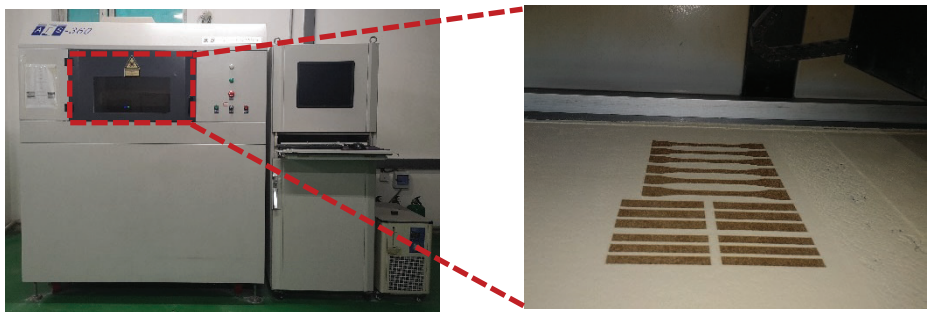

(a) (b)

Figure 4 AFS-360 rapid prototyping machine and LS tests of P-PLA composites

2.3 Characterization methods

Thermal transition temperatures for PLA 3052D powder and P-PLA composites were assessed using a Pyris-Diamond differential scanning calorimeter (DSC) fabricated by PerkinElmer Co., Ltd. For these experiments, the heating rate was set at 10℃/min over the temperature range of 40-240°C. Meanwhile, the thermal decomposition temperature of PLA 3052D powder and pine powder were evaluated using a Pyris 6 TGA. For this testing, the temperature increased from 40°C to 600°C at a heating rate of 10° C/min.

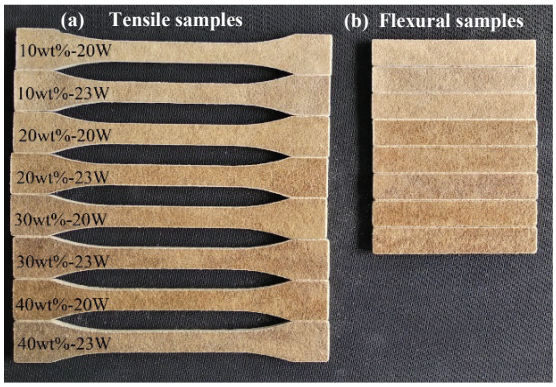

Figure 5 Testing samples of mechanical properties

A microcomputer controlled universal testing machine was used for measuring mechanical properties. Dumbbell shaped tensile specimens (**Figure 5** (a)) with a typical dimension of 150 mm×10 mm×4 mm were fabricated for tensile testing. The crosshead speed was 5 mm/min according to ISO 527-1. Thin specimens of 80 mm×10 mm×4 mm (**Figure 5** (b)) were tested to obtain flexural strength of laser-sintered parts according to the 3-point bending method of ISO 178: 2001. The support span was 52 mm, crosshead speed was 2 mm/min, and midspan deflection was 15 mm.

Microstructures of neat powders and cross-sections of laser-sintered parts were observed by SEM to observe particle features, the binding mechanism, fracture surface and so on. All the specimens were sputtered with a thin layer of gold to eliminate electrical charging prior to SEM observation.

SRZ-400E melt flow rate testing equipment was used to investigate the flowability of PLA 3052D and P-PLA composites over the temperature range 150-165°C with a load of 2.16 kg according to ISO1133-2005. The diameter and length of the device flow channel were 2.095mm±0.005mm and 8.00mm±0.025mm, respectively. Testing materials in the charging barrel were preheated for 10 minutes before the test began.

The density of laser sintered parts was calculated using a mensuration technique based on equation (1). During the density test, different laser sintered part weight was measured using an automatic analytical balance [EBJ-200], and dimensions were measured using a vernier caliper.

$$\rho = \frac{W}{l \cdot d \cdot h} \tag{1}$$

(ρ is density of the part (g/cm^3), W is weight of the part (g), l is length of the part (cm), d is width of the part (cm), h is the thickness of the part (cm)).

3. Results and discussion

Figure 6 (a) depicts thermal phase transition of PLA 3052D, 20 wt.% P-PLA and 30 wt.% P-PLA. Glass transition temperature (T_g) of PLA 3052D is observed at 65°C, and its crystallization temperature (T_{cc}) is 109°C. According to relevant theory [24-26], both the less-ordered α' form crystal and more-ordered α form crystal exist in PLA 3052D when the crystallization temperature is 100-120°C. The bimodal endothermic melting peak is attributed to the melting of the α structure [27]. The lower-temperature peak of 150°C refers to the synchronous melting of the original α-form crystal and to the α'-to-α crystalline phase transition in a melt-recrystallization process. Meanwhile, the higher-temperature peak of 154°C is related to the melting of α crystal formed during the α'-to-α crystalline phase transition [28]. The melting temperature (T_m) of PLA 3052D at 150-154°C is lower than that of neat PLLA or PDLA (T_m is 170-180°C) [29] and stereo-complex crystallite PDLA (T_m is 220-230°C) [30]. As a result, PLA 3052D is prone to easy processing without high heating temperature. As can be seen from DSC curves of 20 wt.% P-PLA and 30 wt.% P-PLA, pine powder loading has almost no effect on the T_{cc} and T_m of P-PLA composites, and only when pine powder loading accounts for 30 wt.% does the T_g of P-PLA composite decline to 61°C. Accordingly, for both PLA 3052D and P-PLA, the same sintering window [123°C - 140°C] for LS processing is determined by the beginning of recrystallization and the beginning of the melting temperature. Combined with the results of LS tests of PLA 3052D, a proper preheating temperature was set at 135-140°C, and the processing temperature was 130-135°C.

The TG curves of PLA 3052D and pine powder are represented in **Figure 6** (b). It indicates that the thermal decomposition temperature (T_d) of PLA 3052D is approximately 300℃. There is a sharp weight loss between 330℃ and 385℃. PLA 3052D decomposed completely above 400℃. Thermal decomposition of pine powder begins at approximately 275℃, a little lower than that of PLA 3052D. That is, pine powder loading may decrease the thermal stability of P-PLA composites. However, higher temperature above 600℃ is needed to burn off the pine powder.

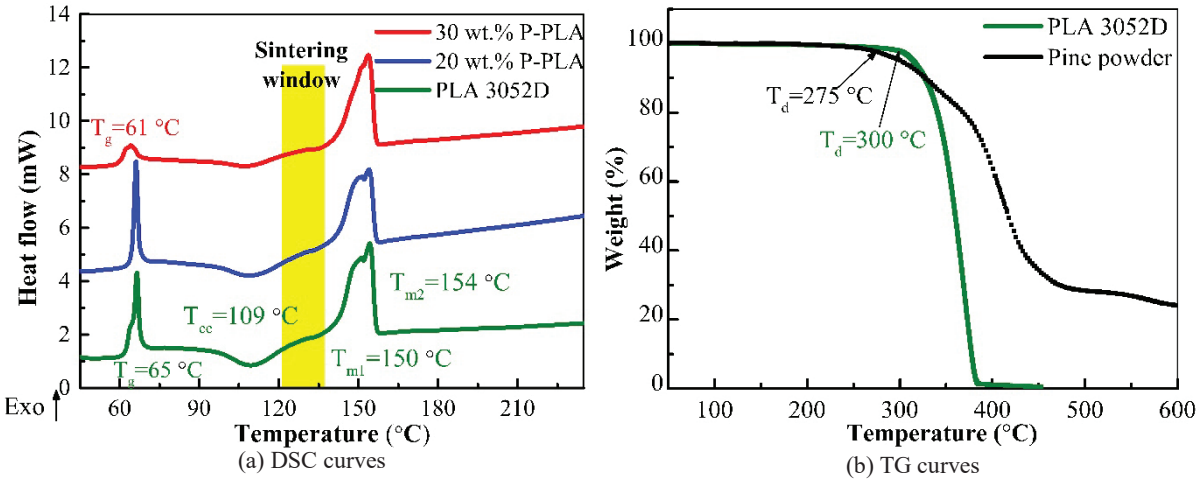

(a) DSC curves (b) TG curves

Figure 6 Thermal behaviors of P-PLA composite and its ingredients

Figure 7 depicts the morphology of laser-sintered PLA 3052D parts under the varying processing temperatures and different laser powers (scanning space 0.2mm, scanning speed 2.0 m/s). With relative low heat input, it is thought that most parts of PLA 3052D remained in solid-state sintering with less partial melting, and PLA particles consolidated together near their original location. Hence, the corresponding laser-sintered parts look white, and shrinkage and deformation of the parts is not apparent. As both processing temperature and laser power increase, less-ordered α' crystals in the PLA will transform into ordered α' crystal form along with lattice deformation. Macroscopically, most part of PLA 3052D particles tend to be melted and recrystallized during LS processing, causing noticeable shrinkage of the whole laser-sintered part and curling at the part's boundary. At the same time, these laser-sintered PLA 3052D parts show improved mechanical properties along with a more semi-transparent appearance.

Figure 7 Morphology of Laser-sintered neat PLA parts

Table 1 records the melt flow index (MFI) of neat PLA 3052D and P-PLA in different mass ratios at 150-165℃. Generally, melt fluidity of PLA 3052D, 10 wt.% P-PLA, 20 wt.% P-PLA, 30 wt.% P-PLA improves with the increase of the heating temperature. For P-PLA composites, the MFI decreases with increasing pine powder loading from 10-40 wt.%. It is thought that the materials' melt shear viscosity and component compatibility account for the observed dependence of MFI on temperature and amount of pine powders. Lots of studies [31-34] prove that the melt viscosity of polymer-based composites, within certain conditions, decreases with increasing temperature, leading to better melt flowability as well as higher melt flow index. Besides, the non-molten pine powders increase the melt viscosity of P-PLA, causing a lower MFI with the increasing amount of pine powders[35-38].

Table 1 Melt flow index of PLA 3052D and P-PLA composites

Powder materials	Melt flow index (The average value, g/ 10 min@2.16Kg)						
	150.0℃	152.5℃	155℃	157.5℃	160.0℃	162.5℃	165.0℃
Neat PLA 3052D	0.21	0.26	7.50	13.63	17.26	23.52	24.96
10 wt.% P-PLA	0.17	0.23	8.70	12.47	16.01	21.88	22.34
20 wt.% P-PLA	0	0.21	8.60	11.25	13.37	20.19	17.46
30 wt.% P-PLA	0	0	1.21	3.86	7.59	10.13	9.42
40 wt.% P-PLA	0	0	0	0	0	0.22	n/a

Noteworthily, the highest MFI of P-PLA composites with 20-40wt.% of pine powders is at 162.5℃, which means their MFI decreases at 165℃. Besides, 40 wt.% P-PLA has almost no melt fluidity. The results are probably due to the poor compatibility between non-polar material (PLA 3052D) and polar material (pine powder), as well as the enlarged difference of melt flowability between PLA and pine powder at high temperature.The density, tensile strength and flexural strength of laser-sintered parts are listed in **Table 2**. They decrease with the increase of pine powder loading. When pine powder accounts for 30-40 wt.%, laser-sintered P-PLA parts show poor mechanical properties and break easily. P-CoPES composite, a kind of wood-plastic composite, is also studied by our research team as the feedstock of LS. The comparison of mechanical properties between P-PLA and P-CoPES is shown in **Figure 8**. Both tensile strength and flexural strength of laser-sintered PLA 3052D parts are about 3.5 times those of laser-sintered CoPES parts. As the matrix of the composite, the performance of either PLA 3052D or CoPES plays a vital role on the mechanical properties of the corresponding wood-plastic composite when pine loading varies between 5-20 wt.%. Laser-sintered P-PLA parts have much better mechanical properties than laser-sintered P-CoPES parts. However, when pine loading is above 30 wt.%, mechanical strength of laser-sintered parts of P-PLA and P-CoPES drops dramatically compared with that of neat polymers. These parts are no longer suitable for service in structural applications.

Table 2 Mechanical properties of laser-sintered P-PLA parts in different mass ratios

Laser-sintered parts （content of pine powder wt.%）	0	10	20	30	40
Density of parts (g/cm^3)	1.11	0.82	0.78	0.56	0.47
Tensile strength (MPa)	23.02	11.76	5.73	1.92	0.78
Flexural strength (MPa)	48.03	22.05	11.90	2.88	1.00

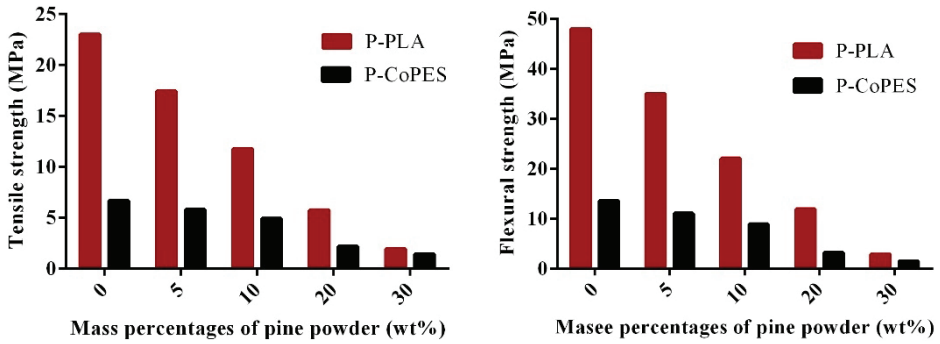

(a) Tensile strength (b) Flexural strength

Figure 8 A comparation of mechanical properties of laser-sintered parts between P-PLA and P-CoPES

The decrease in mechanical properties of laser-sintered P-PLA parts with the increase of pine powder loading can be explained by their microstructural morphology. As can be seen in **Figure 9** (a), laser-sintered PLA 3052D parts are relatively dense, PLA particles are almost fully melted, and some closed pores exist but are less than 50 μm. Some round pits can be seen in laser-sintered parts of PLA 3052D and 10 wt.% P-PLA, which may be due to vapor formation in PLA generated during LS processing, when the mixture is not fully dried or when it absorbs moisture from the environment. For laser-sintered parts of P-PLA (**Figure 9** (b)-(d)), more pores and unclosed channels appear with the increasing amount of pine fibers especially when pine powder accounts for 20-30 wt.%. As a consequence, the laser-sintered P-PLA parts are porous.

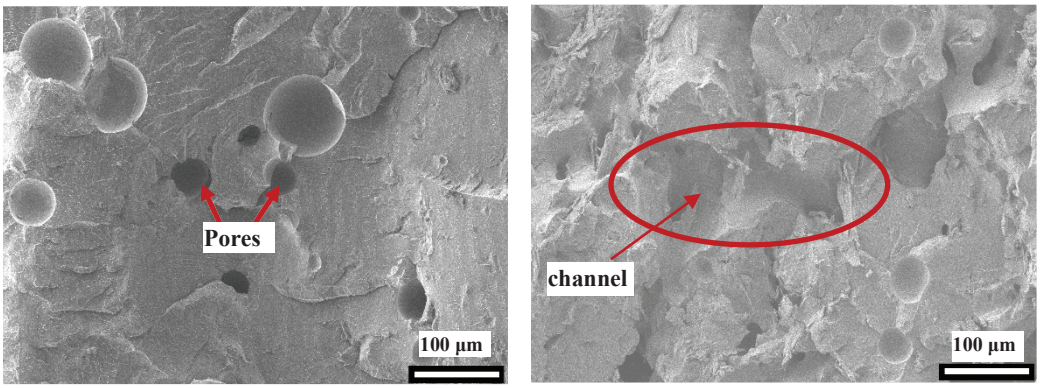

(a) PLA 3052D (b) 10 wt.% P-PLA

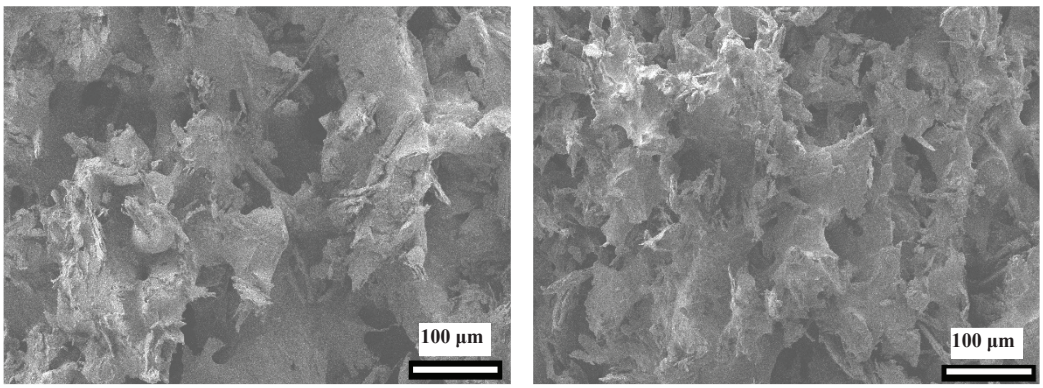

(c) 20 wt.% P-PLA (d) 30 wt.% P-PLA

Figure 9 Microstructures of fracture surfaces of laser-sintered neat PLA parts and P-PLA parts (×100 times)

The situation of mechanical performance and morphology of laser-sintered P-PLA parts can be correlated with the trend observed in the MFI values as a function amount of pine powders. The viscosity of the melt increases with increasing amount of pine thus the MFI decreases. This would also mean that the coalescence and sintering kinetics of the polymers would be retarded with such that the pores and channels are not filled.

On the other hand, as the motion of melt PLA particles is limited due to the resistance from pine fibers, the shrinkage and residual stress generated from solidification of melt PLA will also be reduced along with more pine powder supporting the part structure. Visibly, the deformation of laser-sintered P-PLA parts decreases.

Table 3 lists the dimensional relative error value in the X-Y plane and the Z directions of laser-sintered P-PLA parts with differing amounts of pine powder loadings, compared to the computer solid model. The calculation of relative error value was based on the formula: $V_{relative\ value} = \frac{R_{actual\ value} - R_{ideal\ value}}{R_{ideal\ value}} \times 100\%$. For the results, '+' means dimensional expansion, '–' means dimensional shrinkage. Results in Table 3 show that pine powder helps to reduce the shrinkage of the laser-sintered parts. It shows that 30 wt.% P-PLA has the lowest relative error value in the X-Y plane and 40 wt.% P-PLA has the lowest relative error value in the Z direction.

Table 3 The dimensional relative errors of laser-sintered PLA 3052D and P-PLA parts

Laser-sintered parts （content of pine powder wt.%）		0	10	20	30	40
Relative error value (%)	The X-Y plane	-4.0	-2.27	-0.85	-0.31	-2.15
	The Z direction	-3.25	+0.63	+2.25	+2.25	+0.13

4. Conclusions

Pine-PLA 3052D (P-PLA) parts in different mass ratios were successfully manufactured using laser sintering (LS) technology. P-PLA composite is a type of fully-degradable, nontoxic, environmentally friendly wood-plastic composite which meets the needs of sustainable development. A proper range of processing parameters for laser sintering P-PLA composite were obtained according to the thermal characteristics of the mixture and LS tests. The effects of pine powder loading on the forming properties of laser-sintered P-PLA parts were investigated, and the results show that the pine powder loading improves layer surface flatness during the process of transferring P-PLA composite from the device feed cylinder to the work bed. Meanwhile, the deformation of laser-sintered parts caused by the shrinkage and curling of PLA 3052D declined with increasing additions of pine powder. However, the melt flowability of P-PLA composite and mechanical strength of laser-sintered parts were weakened as the pine loading increased. There is a need to look for a balance between dimensional accuracy and mechanical properties for P-PLA composites according to specific applications.

At the same time, it is essential to improve the morphology and size of P-PLA particles as well as the compatibility of the two ingredients. A series of theoretical combined practical studies should be carried out to optimize the performance of laser-sintered P-PLA parts such as the mechanical properties, the surface quality and dimensional accuracy. The project of laser sintering

of P-PLA is still facing opportunities and challenges before PLA-based WPC is widely used as a commercial feedstock for LS.

5. Acknowledgements

This work was supported by the National Key R&D Program of China (2017YFD0601004), the Fundamental Research Funds for the Central Universities (grant number 2572018AB27, 2572018BF04, 2572017BB07), and also by China Scholarship Council in 2018.

Reference

[1] D.L. Bourell, J.J. Beanman. Powder Material Principles Applied to Additive Manufacturing. Materials Processing and Interfaces TMS (The Minerals, Metals & Materials Society). 1 (2012), 538-544.
[2] W. Zeng, Y. Guo, K. Jiang, Z. Yu, Y. Liu, Y. Shen, J. Deng, P. Wang. Laser intensity effect on mechanical properties of wood–plastic composite parts fabricated by selective laser sintering. J THERMOPLAST COMPOS. 26 (2011), 125-136.
[3] D.L. Bourell, M.C. Leu, K. Chakravarthy, N. Guo, K. Alayavalli. Graphite-based indirect laser sintered fuel cell bipolar plates containing carbon fiber additions. CIRP Annals. 60 (2011), 275-278.
[4] X. Wang, M. Jiang, Z. Zhou, J. Gou, D. Hui. 3D printing of polymer matrix composites: A review and prospective. COMPOS PART B-ENG. 110 (2017), 442-458.
[5] S. Singh, V.S. Sharma, A. Sachdeva, S.K. Sinha. Optimization and Analysis of Mechanical Properties for Selective Laser Sintered Polyamide Parts. MATER MANUF PROCESS. 28 (2013), 163-172.
[6] D. Bourell, J.P. Kruth, M. Leu, G. Levy, D. Rosen, A.M. Beese, A. Clare. Materials for additive manufacturing. CIRP Annals. 66 (2017), 659-681.
[7] K.Y. Jiang, Y.L. Guo, W.L. Zeng, Z.S. Xin. The Preparation of WPC for SLS Rapid Prototyping and Manufacturing. Advanced Materials Research. 113-116 (2010), 1722-1725.
[8] Y. Guo, K. Jiang, D.L. Bourell. Preparation and laser sintering of limestone PA 12 composite. POLYM TEST. 37 (2014), 210-215.
[9] Z. Wu, J. Zhao, W. Wu, P. Wang, B. Wang, G. Li, S. Zhang. Radial Compressive Property and the Proof-of-Concept Study for Realizing Self-expansion of 3D Printing Polylactic Acid Vascular Stents with Negative Poisson's Ratio Structure. MATERIALS. 11 (2018), 1357.
[10] A. Gremare, V. Guduric, R. Bareille, V. Heroguez. Characterization of printed PLA scaffolds for bone tissue engineering. J BIOMED MATER RES A. 106 (2018), 887-894.
[11] Y. Tao, H. Wang, Z. Li, P. Li, S.Q. Shi. Development and Application of Wood Flour-Filled Polylactic Acid Composite Filament for 3D Printing. MATERIALS. 10 (2017), 339.
[12] G. Cicala, D. Giordano, C. Tosto, G. Filippone, A. Recca, I. Blanco. Polylactide (PLA) Filaments a Biobased Solution for Additive Manufacturing: Correlating Rheology and Thermomechanical Properties with Printing Quality. MATERIALS. 11 (2018), 1191.
[13] T. Patrício, M. Domingos, A. Gloria, U. D'Amora, J.F. Coelho, P.J. Bártolo. Fabrication and characterisation of PCL and PCL/PLA scaffolds for tissue engineering. RAPID PROTOTYPING J. 20 (2014), 145-156.
[14] T. Serra, M. Ortiz-Hernandez, E. Engel, J.A. Planell, M. Navarro. Relevance of PEG in PLA-based blends for tissue engineering 3D-printed scaffolds. Materials Science and Engineering: C. 38 (2014), 55-62.
[15] K.F. Leong, C.K. Chua, W.S. Gui, Verani. Building Porous Biopolymeric Microstructures for Controlled Drug Delivery Devices Using Selective Laser Sintering. The International Journal of Advanced Manufacturing Technology. 31 (2006), 483-489.
[16] K.H. Tan, C.K. Chua, K.F. Leong, C.M. Cheah, W.S. Gui, W.S. Tan, F.E. Wiria. Selective laser sintering of biocompatible polymers for applications in tissue engineering. BIO-MED MATER ENG. 15 (2005), 113.
[17] W.Y. Zhou, S.H. Lee, M. Wang, W.L. Cheung, W.Y. Ip. Selective laser sintering of porous tissue engineering scaffolds from poly(l-lactide)/carbonated hydroxyapatite nanocomposite microspheres. Journal of Materials Science: Materials in Medicine. 19 (2008), 2535-2540.
[18] J. Bai, R.D. Goodridge, R.J.M. Hague, M. Okamoto. Processing and characterization of a polylactic acid/nanoclay composite for laser sintering. POLYM COMPOSITE. 38 (2017), 2570-2576.

[19] S.A. Hinchcliffe, K.M. Hess and W.V. Srubar. Experimental and theoretical investigation of prestressed natural fiber-reinforced polylactic acid (PLA) composite materials. Composites Part B: Engineering. 95(2016), 346-354.
[20] V.K. Balla, K.H. Kate, J. Satyavolu, et al. Additive manufacturing of natural fiber reinforced polymer composites: Processing and prospects. Composites Part B: Engineering. 174(2019), 106956.
[21] B. Xu, S. Yin, Y. Wang, et al. Long-fiber reinforced thermoplastic composite lattice structures: Fabrication and compressive properties. Composites Part A: Applied Science and Manufacturing. 97(2017), 41-50.
[22] I. Fidan, A. Imeri, A. Gupta, et al. The trends and challenges of fiber reinforced additive manufacturing. The International Journal of Advanced Manufacturing Technology. 102(2019), 1801-1818.
[23] Phattanaphibul Thittikorn, Opaprakasit Pakorn, and Koomsap Pisut. Preparing Biodegradable PLA for Powder-Based Rapid Prototyping. The 8th Asia Pacific Industrial Engineering & Management System. Taiwan. (2007).
[24] S. Huang, H. Li, S. Jiang, X. Chen, L. An. Crystal structure and morphology influenced by shear effect of poly(l-lactide) and its melting behavior revealed by WAXD, DSC and in-situ POM. POLYMER. 52 (2011), 3478-3487.
[25] K. Wasanasuk, K. Tashiro. Structural Regularization in the Crystallization Process from the Glass or Melt of Poly(l -lactic Acid) Viewed from the Temperature-Dependent and Time-Resolved Measurements of FTIR and Wide-Angle/Small-Angle X-ray Scatterings. MACROMOLECULES. 44 (2011), 9650-9660.
[26] Y. Yin, G. Liu, Y. Song, X. Zhang, S. de Vos, R. Wang, C.A.P. Joziasse, D. Wang. Formation of stereocomplex in enantiomeric poly(lactide)s via recrystallization of homocrystals: An in-situ X-ray scattering study. EUR POLYM J. 82 (2016), 46-56.
[27] T. Tábi, A.F. Wacha, S. Hajba. Effect of D‐lactide content of annealed poly(lactic acid) on its thermal, mechanical, heat deflection temperature, and creep properties. J APPL POLYM SCI. 136 (2018), 47103.
[28] J. Zhang, K. Tashiro, H. Tsuji, A.J. Domb. Disorder-to-Order Phase Transition and Multiple Melting Behavior of Poly(l-lactide) Investigated by Simultaneous Measurements of WAXD and DSC. MACROMOLECULES. 41 (2008), 1352-1357.
[29] J. Shao, S. Xiang, X. Bian, J. Sun, G. Li, X. Chen. Remarkable Melting Behavior of PLA Stereocomplex in Linear PLLA/PDLA Blends. IND ENG CHEM RES. 54 (2015), 2246-2253.
[30] H. Tsuji. Poly(lactic acid) stereocomplexes: A decade of progress. ADV DRUG DELIVER REV. 107 (2016), 97-135.
[31] V. Mazzanti, F. Mollica and N. El Kissi. Rheological and mechanical characterization of polypropylene-based wood plastic composites. Polymer Composites. 37(2016), 3460-3473.
[32] C.M. Cobos, L. Garzon, J.L. Martinez, et al. Study of thermal and rheological properties of PLA loaded with carbon and halloysite nanotubes for additive manufacturing. Rapid Prototyping Journal. 25(2019), 738-743.
[33] V. Speranza, A. D. Meo and R. Pantani. Thermal and hydrolytic degradation kinetics of PLA in the molten state. Polymer Degradation and Stability. 100(2014), 37-41.
[34] M. Fujiyama and M. Kondou. Effect of gelation on the flow processability of poly(vinyl chloride). Journal of Applied Polymer Science. 90(2003), 1808-1824.
[35] V. Mazzanti and F. Mollica. In-Process Measurements of Flow Characteristics of Wood Plastic Composites. Journal of Polymers and the Environment. 25(2017), 1044-1050.
[36] W. Harnnarongchai, J. Kaschta, D. W. Schubert, et al. Shear and elongational flow properties of peroxide-modified wood/low-density polyethylene composite melts. Polymer Composites. 33(2012), 2084-2094.
[37] M. Golzar, N.J. Jam and A.H. Behravesh. Mathematical and experimental study on flow of wood plastic composite to acquire its constitutive equation. Journal of Reinforced Plastics and Composites. 31(2012), 749-757.
[38] T. Rokkonen, H. Peltola and D. Sandquist. Foamability and viscosity behavior of extrusion foamed PLA‐pulp fiber biocomposites. Journal of Applied Polymer Science. 136(2019), 48202.